Effect of Spatial Resolution on SPECT Quantification Values

Akihiro Kojima, Masanori Matsumoto, Mutsumasa Takahashi, Yoshihisa Hirota, and Hideteru Yoshida

Department of Radiology, Kumamoto University, School of Medicine, Kumamoto 860, Japan; and College of Medical Science, Kumamoto University, Kumamoto 862, Japan

The effect of spatial resolution on quantification by single photon emission computed tomography (SPECT) was studied using a rotating gamma camera and ^{99m}Tc. Using phantoms with hot and cold regions, experiments were performed to ascertain relationships between the source and the SPECT image, and to compare them with theoretic calculations. According to the results, the SPECT value represented the true radioactivity when the objects' sizes were 2.5 times larger than full width at half maximum (FWHM) for hot regions. For cold regions, there were errors of ~20% for the true value, even in the case of such large sizes. In addition, sizes at half maximum images corresponded to true object sizes when hot region sizes were larger than 1.4 × FWHM. The relationship between absolute radioactivity and total SPECT value was linear when the threshold level was zero. Knowing the effect of spatial resolution is a necessity in clinical SPECT studies.

J Nucl Med 30:508–514, 1989

Single photon emission computed tomography (SPECT) has been used for three-dimensional displays of radioactive distributions and for estimating volumes within the body (*1,2*). However, SPECT values do not always represent true radioactive concentrations, thus quantitative analyses are rendered unreliable. These facts can be explained by several factors, such as projection data acquisition, reconstruction of transverse images, absorption correction, Compton scattering, energy resolution, and image noise (*3–5*). Limited spatial resolution, which is dependent on source-detector distance, may also play a role.

The effect of spatial resolution was studied for positron emission tomography (PET) (*6–8*). It has been shown that object sizes obtained with true radioactive concentrations were 2 × full width at half maximum (FWHM), 2.4 × FWHM, and 2.7 × FWHM for one-, two-, and three-dimensional objects for hot regions (*8*). For SPECT, the relationships of the recovery coefficient (RC) to the hot source area were studied for various collimators and image reconstruction filters, using technetium-99m (^{99m}Tc) and indium-131 (^{131}I)(*9*).

This study investigated the effect of spatial resolution on quantification of radioactive concentrations in SPECT images, using phantoms with hot and cold regions. Special attention has been devoted to the relationships between object size and SPECT value, object size and image size, and the absolute radioactivity and total SPECT value compared with theoretic calculations.

Received May 9, 1988; revision accepted Dec. 23, 1988.

For reprints contact: Akihiro Kojima, MSc, Dept. of Radiology, Kumamoto University, School of Medicine, 1-1-1 Honjo, Kumamoto 860, Japan.

MATERIALS AND METHODS

Data Acquisition

A SPECT system (ZLC-37-ECT, Siemens, Gammasonics, Inc., Des Plaines, IL) with a rotating gamma camera was used with a low-energy, high resolution, parallel hole collimator. This system was interfaced with a nuclear medicine computer (Scintipac 2400, Shimadzu, Co., Ltd., Kyoto, Japan). The energy window was set at 140 keV ± 10% for ^{99m}Tc. All sets of projection data consisted of 64 view images over 360°. Following acquisition, reconstruction of transverse images was performed using the backprojection method and Shepp and Logan convolution filter (*10*) without correction for absorption. The image matrix for acquisition and reconstruction was 64 × 64. The size of each pixel and slice thickness were 6 mm.

Phantom

Two phantoms were used in this study.

Phantom 1: Phantom for measuring the point spread function (PSF). A line source (0.6 mm in diameter, 16 cm long), containing 74MBq of ^{99m}Tc, was imaged in a water-filled cylindrical container (20 cm in diameter, 20 cm long). The

total cts/slice and maximum-ct/pixel were 8×10^4 and 2×10^3, respectively. That source was placed parallel to the central axis of the container 5 cm off the axis. The central axis of the container was on the camera's rotation axis. The radius of rotation was changed to 15 cm, 20 cm, and 25 cm. Each FWHM of PSF was measured from the corresponding transverse images, using interpolation.

Phantom 2: Phantom for hot and cold spots. To obtain images of hot and cold spots, two phantoms were used. One consisted of four cylinders, each 5 cm in length and 5mm, 15 mm, 25 mm, and 35 mm in diameter located 90° apart, 5 cm off the axis. The other phantom consisted of four cylinders, each 5 cm in length and 10 mm, 20 mm, 30 mm, and 40 mm in diameter located 90° apart, and 5 cm off the axis. The two phantoms were placed in a water-filled cylindrical container, 20 cm in diameter and 20 cm in length, together and imaged with the axis of rotation coinciding with the axis of the container. Hot spot images were reconstructed with each of the eight cylinders having a uniform radioactive concentration (370 kBq/ml of ^{99m}Tc) and no background. There were totals of 2×10^5 counts and a maximum of 2×10^3 cts/pixel in the reconstructions. Cold spot imaging was performed without filling the eight cylinders with radioactive water, and with warm background (740 kBq/ml of ^{99m}Tc). The total counts and maximum-ct/pixel in the reconstructions were 6×10^5 and 10^3, respectively.

Data Analysis

Scan data were analyzed in the following manner.

Hot spot image. For images of objects larger than FWHM, the mean count of a few pixels surrounding the maximum was taken for smaller objects, only the maximum was taken as the SPECT value. These values, normalized by the value (2,000 counts) for the largest object (40 mm i.d), were termed "relative SPECT values" and plotted against the object size. Moreover, to determine the relationship between object size and image size, the diameter at half maximum (DHM) and the diameter at tenth maximum (DTM) of hot spot images corresponding to FWHM and FWTM, respectively, were measured. Total SPECT values in the region of interest (ROI) at the threshold level (TL) were also obtained for estimating the absolute radioactivity. These values were normalized by total counts (60,000) of the area of 400 π mm^2 source-50% TL and were termed "relative total SPECT values (RTV)".

Cold spot image. The ratio of the difference between the minimum SPECT value/pixel in a cold spot image (V_{min}) and background value/pixel (V_{bg}) to V_{bg} was defined as the contrast value/pixel (C_s),

$$C_s = |V_{min} - V_{bg}|/V_{bg}. \quad (1)$$

The relationship between the object size and C_s was similarly obtained. Theoretically, C_s is equal to the relative SPECT value in a hot spot image.

Theoretic Calculation

A theoretic calculation was performed to compare the data with experimental results. On the x,y plane, we approximated PSF to the Gaussian function,

$$F(x, y) = G \exp[-k(x^2 + y^2)/R^2], \quad (2)$$

where R is the same FWHM obtained from the experimental data, and G and k are constant and defined as the volume of PSF in unity [$G = k^2/(4 \pi R^2)$]. If the area and the distribution of the radioactivity in a cylindrical source are S and A(x,y), respectively, the observed response C(x,y) is represented by the convolution integral of A(x,y) with F(x,y);

$$C(x, y) = \int \int s\, A(x, y) F(x - X, y - Y)\, dX\, dY. \quad (3)$$

Equation (3) was solved by a numeric integration algorithm using a minicomputer (Scintipac 2400).

RESULTS

Spatial Resolution

Three PSFs were obtained by changing the radius of rotation to 15 cm, 20 cm, and 25 cm. Three FWHMs were measured from these PSFs, and they were 14.5 mm, 16.5 mm, and 18.5 mm, respectively. Half profiles of the PSF's images, which were normalized according to the maximum SPECT value, are shown in Figure 1. As the theoretic PSF, the Gaussian functions with the same FWHM as the experimental data, are also indicated by the solid line. All three profiles are similar.

Calculation

The observed response C(x,y) for cylindrical sources having various sizes was calculated from Eq. (3), letting A(x,y) be constant and changing FWHM to 14.5 mm, 16.5 mm, and 18.5 mm. Figure 2 shows six profiles of C(x,0) when FWHM = 14.5 mm. Although all radioactive concentrations of the six sources are equal, the maximum values of a calculated profile for the smaller objects are low. When the diameter of a cylinder is larger than 40 mm, the maximum value of a profile becomes equal to the true value.

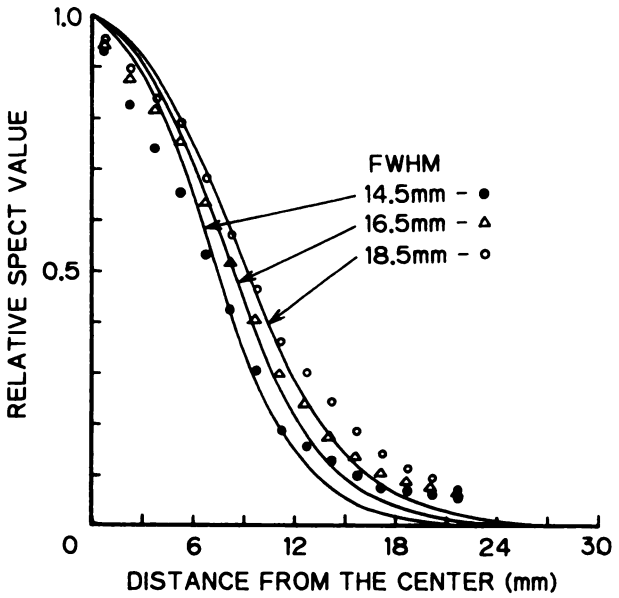

FIGURE 1
Point spread functions obtained by the experiment and the theoretic calculation (solid lines) with the same FWHMs.

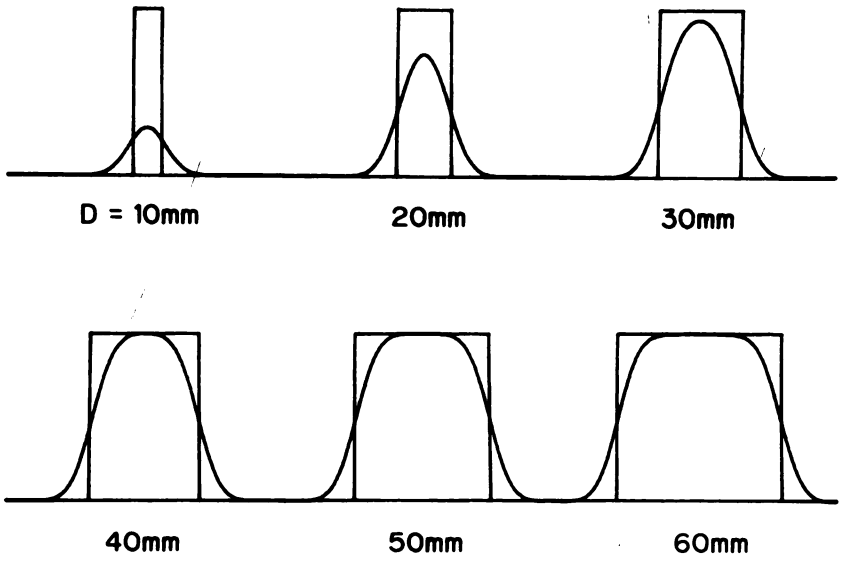

FIGURE 2
Simulated SPECT data of hot spot objects with the various diameters (D) for FWHM = 14.5 mm. These show profiles of perpendicular planes through the center of images. Rectangles are drawn together as the true profiles of objects.

Effect of Spatial Resolution

The transverse images for hot or cold spot objects are shown in Figure 3. Although all hot spot objects truly have the same radioactive concentration, the smaller objects are underestimated compared with the larger objects (Fig. 3A). For cold spot objects (no radioactivity), although the center of that image is low because of no absorpition correction, the smaller objects show poor contrast (Fig. 3B). Numeric data obtained from various images are plotted in Figures 4 and 5, and compared with the theoretic calculations. For the hot spot images, the experimental data are in good agreement with the calculated data. Figure 4B shows that the object size which represents the true radioactive concentration is more than 2.5 × FWHM. The relative SPECT values become 0.8, 0.5, and 0.15 for the object sizes 2 × FWHM, 1 × FWHM, and 0.5 × FWHM, respectively. On the contrary, the contrast value does not reach the true value even if the cold spot size is very large, with an error of ~20% (Fig. 5B). Furthermore, for smaller objects the contrast value by experiment is better than the value from calculations.

The relationship between the diameter of an object and DHM or DTM as obtained from the hot spot images are indicated in Figure 6. If the diameter of an object (D) is larger than 20mm (1.4 × FWHM), DHM becomes equal to D. However, DTM is not equal to D, even if D is very large.

The relationship between the absolute radioactivity and the total SPECT value is shown in Figure 7. The hot spot object area represents the absolute radioactivity if the radioactive concentration is known. The threshold level (TL) values are changed from 0% to 90%. When TL is only zero, RTV has a linear relationship with the object area. With increasing TL, however, it becomes nonlinear at the smaller object area.

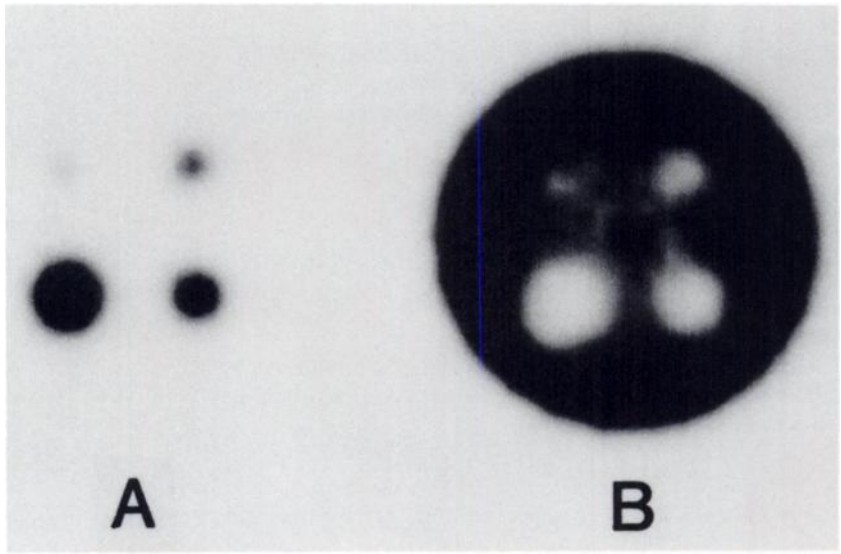

FIGURE 3
Transverse images obtained from experiments of phantoms with four cylinders (10 mm, 20 mm, 30 mm, and 40 mm) for FWHM = 14.5 mm. A: The hot spot image with cold background. The smaller objects are underestimated. B: The cold spot image with warm background. The smaller objects are overestimated.

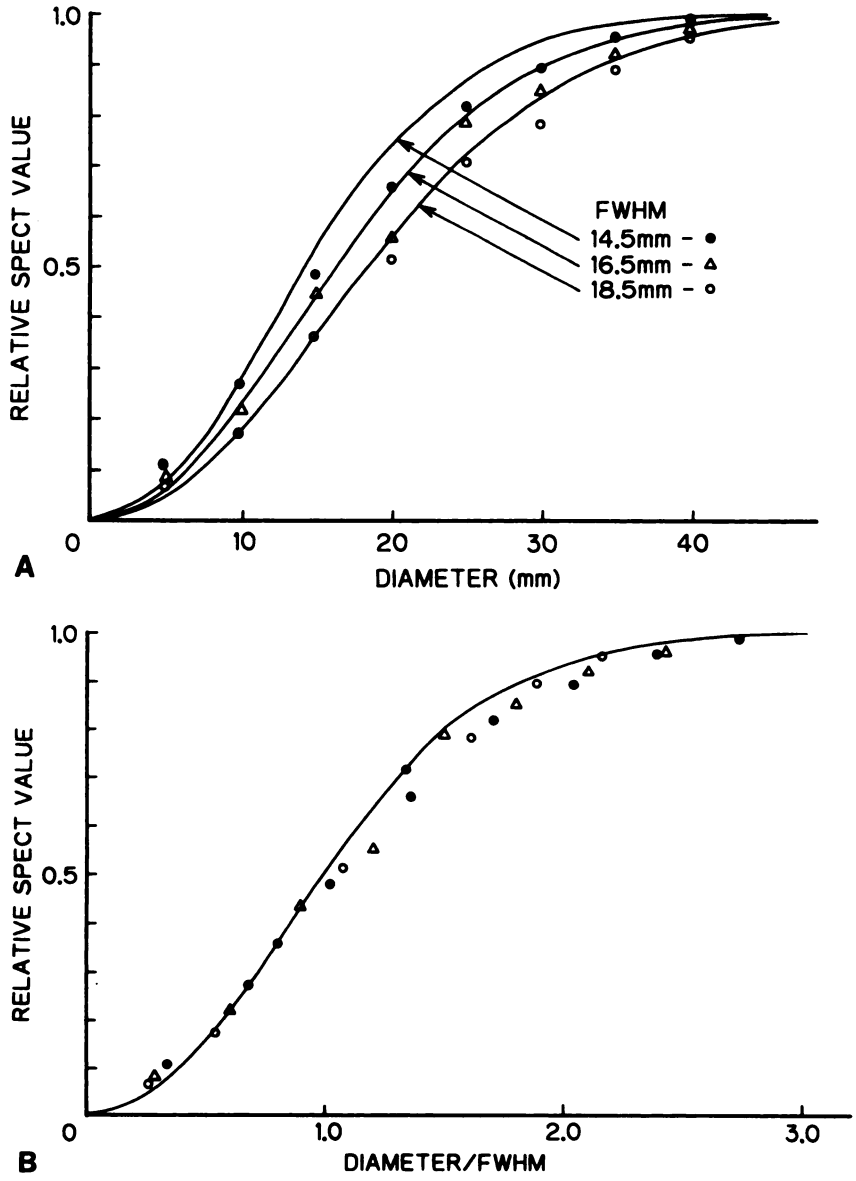

FIGURE 4
Relationship between the hot object size (diameter) and the relative SPECT value for three FWHMs. The object size is represented by both the dimension (A) and the normalization on FWHMs (B). The experiment's results are compared with the theoretic calculations (solid lines) and show good agreement.

DISCUSSION

The influence of finite spatial resolution on object size cannot be ignored in quantitative analysis by SPECT. We investigated the effect of spatial resolution on the SPECT value using phantoms, and identified other factors which make quantitative SPECT imaging more difficult than theoretic calculations. These factors have been studied by many investigators. In this report, we do not refer to such factors, but only describe spatial resolution.

The phantoms used in the present study were hot spot phantoms with cold background and cold spot phantoms with warm background. These are essential for the quantitative analysis and suitable for many clinical situations.

For hot spot objects, SPECT values represented the true radioactive concentrations when the object size was 2.5 times larger than FWHM (Fig. 4). Kessler et al. (*8*) reported that for two-dimensional objects, an object size of 2.4 × FWHM is required to obtain 98% recovery. On the contrary, there were two serious differences between the experimental and calculated data for cold spot objects (Fig. 5). First, an underestimate of ~20% of the contrast occurred even when the object size was larger than 2.5 × FWHM. This main factor was because of Compton scatter photons from the surrounding source. Second, contrasts for the smaller objects were better than calculations. This may have been a result of image noise and software error of the reconstruction algorithms. Our results suggest that small objects, such as the myocardium, must be dealt with more carefully. Garcia et al. (*14*) reported comprehensive two-dimensional polar map images representing the distribution of thallium-201 (^{201}Tl) in the myocardium. They used maximal-count circumferential profiles (CP) for each

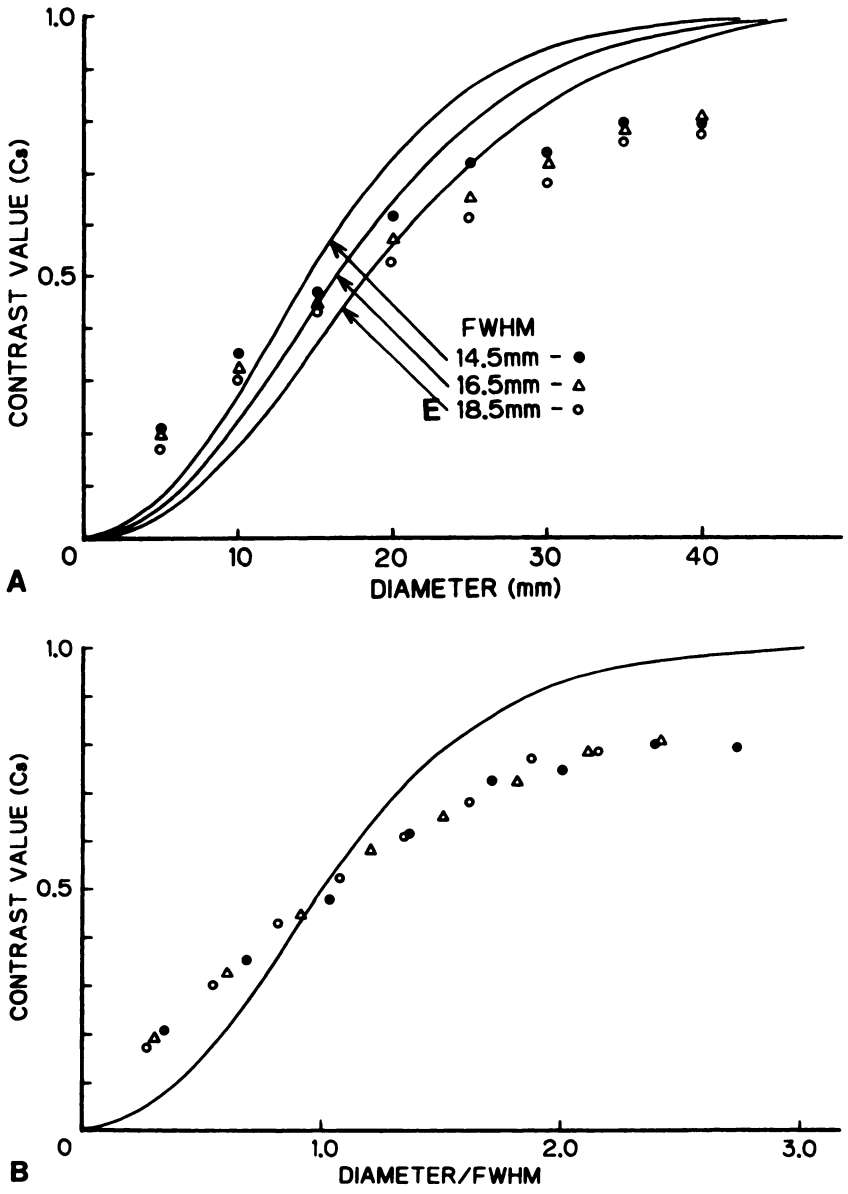

FIGURE 5
Relationship between the cold spot object size (diameter) and the contrast value (C_s) for three FWHMs. The object size is represented by both the dimension (A) and the normalization on FWHMs (B). The experiment's results are compared with the theoretical calculations (solid lines). Notice the difference between the two curves.

short-axis image. Since Figures 4 and 5 show that the thickness of the myocardium and defect size influence the maximum value, careful attention should be afforded when such a CP is used. Caldwell et al. (*15*) and Chan et al. (*16*) discussed overestimates of perfusion defects in myocardial SPECT images of ^{201}Tl. They also referred to the effect of spatial resolution.

Estimating an organ's volume based on areas in tomographic sections is facilitated by SPECT quantification. In determining areas to be imaged, the threshold level (TL) method is often used. Tauxe et al. (*17*) used phantoms to determine the TL of object images for estimating the volume closest to the true volume. They reported excellent correlation when TL was set at 50% for cylindrical phantoms or 45% for ellipsoidal phantoms. Figure 6 shows that the image size of 50%TL represents the true object size when the object size is larger than 1.4 × FWHM. However, when the object size is smaller than this, the image size of 50%TL becomes large and the calculated volume is overestimated. This means that TLs larger than 50% should be used to estimate volumes whose cross section areas are small.

The absolute radionuclide accumulation in the body must be known for clinical diagnosis and radioimmunotherapy. For that purpose the relationship between the absolute radioactivity and the total SPECT value must be linear. Generally, summed counts in the ROI at any TL may be used as a total SPECT value. When TI = 0%; that is, when the ROI completely surrounding the sources is set, the total SPECT value correlates linearly with the absolute radioactivity, regardless of

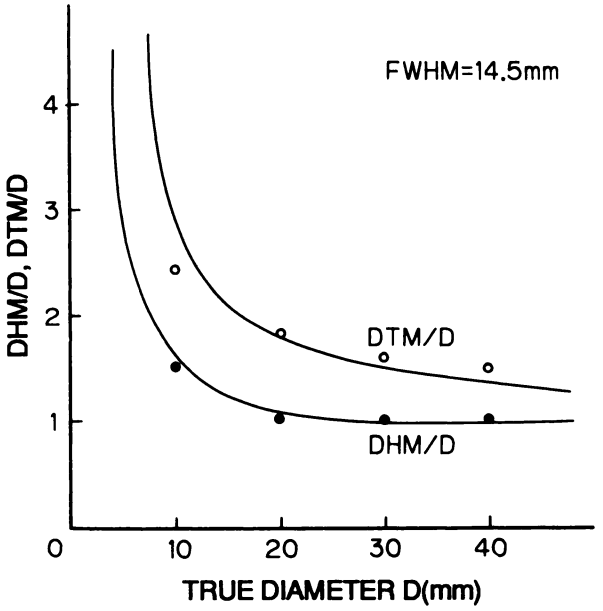

FIGURE 6
Relationship between the hot spot object size (diameter, D) and DHM/D or DTM/D. DHM means the diameter at half maximum and DTM the diameter at tenth maximum in a hot spot image. Solid lines express DHM and DTM from the theoretic calculation.

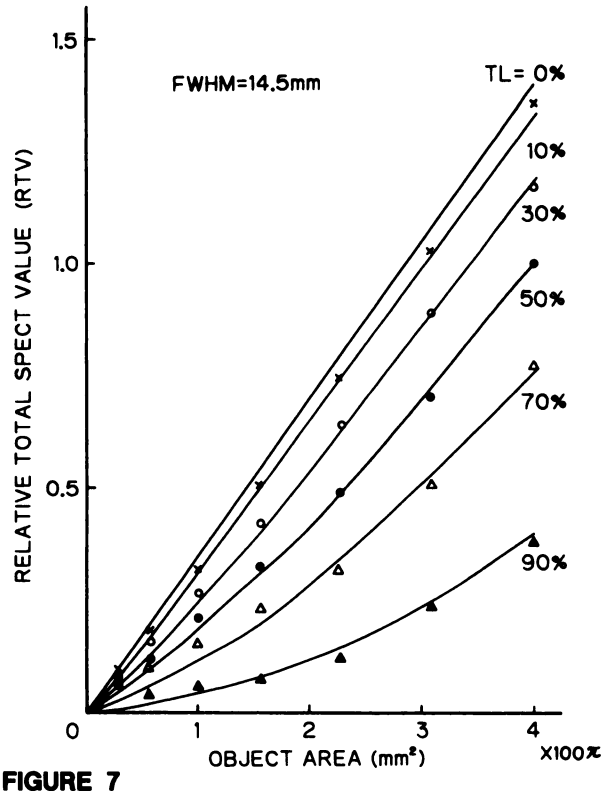

FIGURE 7
Relationship between the hot spot object area and the RTV on varying the TL. The hot spot object area represents the absolute radioactivity if the radioactive concentration is known. When TL is only zero, that relationship becomes linear. Solid lines express RTV from the theoretic calculation.

source size. In clinical SPECT studies, TL = 0% cannot be used because there is background surrounding the source and software artifacts appeared near the source. Then, one must use the higher TL, which is determined empirically. As shown in Figure 7, when TL is higher, the linearity for the smaller object is interrupted. Therefore, more attention must be afforded such smaller objects in order to estimate the absolute radioactivity.

Although we modeled two-dimensional radionuclide perfusion in this study, a three-dimensional model may be better for illustrating the partial volume effect. However, since SPECT quantifications are performed practically using two-dimensional tomographic images, we believe that our phantom experiments and calculations are adequate.

In this way, finite spatial resolution of the system influences the quantitative analysis using SPECT imaging. To improve spatial resolution, smaller pixel size and zooming technique are used for data acquisition and reconstruction. Since SPECT systems have also been improved (*18–20*), it will be possible to visualize smaller objects and perform quantitative analysis for them.

ACKNOWLEDGMENT

The authors thank Walter J. Russell, MD, DMSc of the Radiation Effects Research Foundation, Hiroshima, for editing this manuscript.

REFERENCES

1. Budinger TF, Gullberg GT. Three dimensional reconstruction in nuclear medicine emission imaging. *IEEE Trans Nucl Sci* 1974; NS-21:2–20.
2. Strauss LG, Clorius JH, Frank T, Kaick GV. Single photon emission computerized tomography (SPECT) for estimates of liver and spleen volume. *J Nucl Med* 1984; 25:81–85.
3. Budinger TF. Physical attributes of single-photon tomography. *J Nucl Med* 1980; 21:579–592.
4. Moore SC. Quantitative capabilities of single-photon emission computerized tomography. In: Magistretti PL, ed. *Functional radionuclide imaging of the brain.* New York: Raven Press, 1983:177–192.
5. Soussaline FP, Todd-Pokropek AE, Zurowski S, Huffer E, Raynaud CE, Kellershohn CL. A rotating conventional gamma camera single-photon tomographic system: physical characterization. *J Comp Assist Tomogr* 1981; 5:551–556.
6. Hoffman EJ, Haung SC, Phelps ME. Quantitation in positron emission computed tomography: 1. effect of object size. *J Comp Assist Tomogr* 1979; 3:299–308.
7. Mazziotta JC, Phelps ME, Plummer D, Kuhl DE. Quantitation in positron emission computed tomography: 5. physical-anatomical effects. *J Comp Assist Tomogr* 1981; 5:734–743.
8. Kessler RM, Ellis JR, Jr., Eden M. Analysis of emis-

sion tomographic scan data: limitations imposed by resolution and background. *J Comp Assist Tomogr* 1984; 8:514–522.
9. Clarke LP, Leong LL, Serafini AN, Tyson IB, Silbiger ML. Quantitative SPECT imaging: influence of object size. *Nucl Med Commun* 1986; 7:363–372.
10. Shepp LA, Logan BF. The Fourier reconstruction of a head section. *IEEE Trans Nucl Sci* 1974; NS-21:21–43.
11. Jaszczak RJ, Whitehead FR, Lim CB, Coleman RE. Lesion detection with single-photon emission computed tomography(SPECT) compared with conventional imaging. *J Nucl Med* 1982; 23:97–102.
12. Kircos LT, Carey JE, Jr., Keyes JW, Jr. Quantitative organ visualization using SPECT. *J Nucl Med* 1987; 28:334–341.
13. Chang W, Henkin RE, Buddemeyer E. The sources of overestimation in the quantification by SPECT of uptakes in a myocardial phantom: concise communication. *J Nucl Med* 1984; 25:788–791.
14. Garcia EV, Train KV, Maddahi J, et al. Quantification of rotational thallium-201 myocardial tomography. *J Nucl Med* 1985; 26:17–26.
15. Caldwell JH, Williams DL, Hamilton GW et al. Regional distribution of myocardial blood flow measured by single-photon emission tomography: comparison with in vitro counting. *J Nucl Med* 1982; 23:490–495.
16. Chang W, Henkin RE. Photon attenuation in Tl-201 myocardial SPECT and quantification through an empirical correction. In: Esser PD, ed. *Emission computed tomography: current trends.* New York: The Society of Nuclear Medicine, 1983:123–133.
17. Tauxe WN, Soussaline F, Todd-Pokropek A, et al. Determination of organ volume by single-photon emission tomography. *J Nucl Med* 1982; 23:984–987.
18. Gottschalk SC, Salem D, Lim CB, Wake RH. SPECT resolution and uniformity improvement by noncircular orbit. *J Nucl Med* 1983; 24:822–828.
19. Esser PD, Alderson PO, Mitnick RJ, Arliss JJ. Angled-collimator SPECT (A-SPECT): an improved approach to cranial single photon emission tomography. *J Nucl Med* 1984; 25:805–809.
20. Tsui BMW, Gullberg GT, Edgerton ER, Gilland DR, Perry JR, McCartney WH. Design and clinical utility of a fan beam collimator for SPECT imaging of the head. *J Nucl Med* 1986; 27:810–819.